Chalcogenide Letters Vol. 16, No. 11, November 2019, p. 513 - 522

THERMODYNAMIC PROPERTIES OF $CuAlS_2$ WITH CHALCOPYRITE STRUCTURE FROM FIRST-PRINCIPLES CALCULATIONS

Y. YU*, X. G. KONG, Y. H. SHEN, J. DENG
College of Optoelectronic Engineering, Chengdu University of Information Technology, Chengdu 610225, China

We have performed detailed studies of the lattice dynamics and thermodynamic properties of $CuAlS_2$ within the density functional perturbation theory and pseudopotential methods. The results for the phonon dispersion curves of $CuAlS_2$ along several high-symmetry lines together with the corresponding phonon density of states are given. The thermodynamic properties were derived from phonon frequencies calculated within the quasi-harmonic approximation. The temperature dependence of various quantities such as the free energy F, entropy S, the volume thermal expansion α_V, the heat capacity at constant volume C_V, and the heat capacity at constant pressure C_P are computed. Our results are in good agreement with available experimental data and other calculations.

(Received August 28, 2019; Accepted November 8, 2019)

Keywords: $CuAlS_2$, DFPT, Vibrational, Thermodynamic, QHA

1. Introduction

The chalcopyrite I-III-VI_2 (I=Cu, Ag; III=In, Ga, Al; and VI=S, Se, Te) family crystals have been attracting considerable attention as potential materials for employed in photovoltaic solar-energy production due to their very high absorption coefficient under sunlight [1,2]. Among them, $CuAlS_2$ has been studied for several decades as a promising windows material for solar cells, light-emitting diodes, and other applications because it has the widest direct band gap of 3.49 eV at 300 K [3]. In addition, a previous photoluminescence (PL) experiment revealed that the exciton binding energy of $CuAlS_2$ is 70 meV [4], which is larger than the binding energies of other ultraviolet emitting materials such as GaN, ZnS, and ZnO [5]. This implies that $CuAlS_2$ has the potential to be a highly efficient ultraviolet emitter at room temperature.

The thermodynamic properties are one of the most basic properties of any material and depend on the lattice dynamical behaviour. The lattice dynamical properties of $CuAlS_2$ have been studied for the last four decades by a number of experimental and theoretical methods. Experimentally, the Brillouin zone (BZ) center (Γ point) phonon frequencies of $CuAlS_2$ are measured mainly by Roman spectroscopy [6-8] and a few by infrared spectroscopy [6,7,9-11]. However, measured vibrational properties of $CuAlS_2$ have been limited to the BZ center possibly due to experimental difficulties to make large enough single crystals. On the theoretical side, there have been a few attempts to calculate the lattice dynamical by first-principles methods. Using first-principles density functional theory (DFT) [12,13] and density functional perturbation theory

* Corresponding author: yy2012@cuit.edu.cn

(DFPT) [14,15], Parlak and Eryiğit [16] computed vibrational properties of $CuAlS_2$. Modern first-principles calculation techniques of phonon crystal properties based on DFPT formalism have proven to be an effective research tool. The results of such investigations are highly reliable and have predictive power. Nowadays, first-principles calculations of lattice dynamics of chalcopyrite $CuInSe_2$ [17,18], $CuGaS_2$ [19], $CuGaSe_2$ [20], $CuInS_2$ [21] and $ZnSnP_2$ [22] using DFPT have been reported. Although the phonon frequencies are calculated by Parlak and Eryiğit, the thermodynamic properties of $CuAlS_2$ are not given.

Several calculations have been performed to study the thermodynamic properties of $CuAlS_2$. Verma et al. [23] used the quasi-harmonic Debye model [24] to investigate the thermodynamic properties of $CuAlS_2$ including volume expansion coefficient, bulk modulus, specific heat and entropy. Although this method has been successfully applied for many years, it has limitations in study of anharmonic effects, extreme conditions of temperature and pressure, and temperatures close to the melting point [25]. In 2005, Korzun et al. [26] measured the heat capacity at constant pressure C_P of $CuAlS_2$ and calculated the heat capacity at constant volume C_V, entropy H and enthalpy S from the experimental results using polynomial curve fitting techniques. This method relies on experimental data, and if the measured results are not accurate, the calculation results will have a large deviation.

In this work we will focus on the thermodynamic properties of $CuAlS_2$. Since lattice vibration constitutes main contribution to thermodynamic function of materials at finite temperatures, detailed information on the phonon spectrum is crucial for understanding the thermodynamic properties under finite temperatures. The phonon density of states (PDOS), which includes contributions from all phonon over the entire Brillouin zone, is needed for the calculations of various thermodynamic functions under the harmonic approximation [27,28], e.g. free energy, internal energy, entropy and heat capacity. And thermal expansion behavior can be evaluated from free energy versus volume curves by the method based on the quasi-harmonic approximation (QHA) [27-29].

2. Computational methods

The first-principles calculations are carried out by using VASP (Vienna ab initio Simulation Package) code [30] which is based on the density functional theory [12,13]. The ion-electron interaction is described by the projector augmented wave (PAW) method [31], and the exchange-correlation functional is treated within the Generalized gradient approximation (GGA) [32,33] of PW91 [34]. Herein, the Cu ($3d^{10}$, $4s^1$), Al ($3s^2$, $3p^1$), and S ($3s^2$, $3p^4$) orbital are treated as valence states. The plane-wave cutoff energy for electronic wavefunctions was set at 550 eV. A 2×2×1 supercell was constructed and relaxed with a 3×3×3 k-point mesh for use in structure and lattice dynamics calculations. The iterative process is stopped when all forces acting on each atom are relaxed to be less than 10^{-4} eV/Å and the total energy deviation between two consecutive steps reach to 10^{-6} eV.

The phonon dispersion curves and phonon density of state are determined by using density functional perturbation theory combined with the PHONOPY code [35]. After phonon calculations, finite temperatures thermodynamic properties of $CuAlS_2$ are estimated by the quasi-harmonic approximation. In the quasi-harmonic approximation, the Helmholtz free energy is given by

$$F(V,T) = E(V) + F_{vib}(V,T) \quad (1)$$

where $E(V)$ is the static contribution to the internal energy, and $F_{vib}(V,T)$ represents the vibrational contribution to the free energy, and $F_{vib}(V,T)$ is given by

$$F_{vib}(T,V) = k_B T \sum_{j,q} \ln\left\{2\sinh\left[\hbar\omega_{j,q}(V)/2k_B T\right]\right\} \quad (2)$$

Here, $\omega_{j,q}(V)$ is the phonon frequency of the *j*th phonon mode with wave vector *q* at fixed *V*, and k_B is the Boltzmann constant. The PDOS and vibrational free energy were calculated at several different cell volumes. For $CuAlS_2$, we have performed a series of calculations by changing the lattice constants of the supercells along *a*-axis and *c*-axis directions independently.

3. Results and discussion

3.1 Structural properties

$CuAlS_2$ has the chalcopyrite structure shown in Fig. 1. The lattice is body centered and the space group is $I\bar{4}2d$. The tetragonal unit cell contains four formula units while the primitive cell contains two. It may be seen that the structure resembles that of zinc blende when the atoms on Cu and Al sites are indistinguishable or when the occupation of these sites by Cu and Al is completely random. For $CuAlS_2$, the Cu atom is located at (0, 0, 0), (0, 1/2, 1/4); Al at (0, 0, 1/2), (0, 1/2, 3/4) and S at (*u*, 1/4, 1/8), (-*u*, 3/4, 1/8), (3/4, *u*, 7/8), (1/4, -*u*, 7/8).

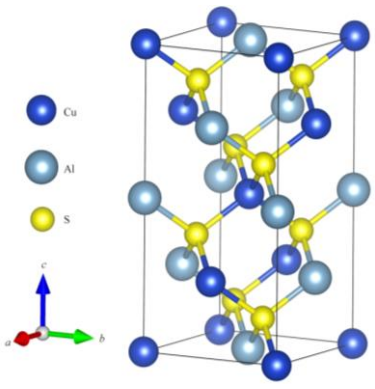

Fig. 1. Crystal structure of $CuAlS_2$.

In general, I-VI and III-VI bond lengths, denoted by $d_{Cu\text{-}S}$ and $d_{Al\text{-}S}$, respectively, are not equal, mentioned substitution results in two different structural deformations. First is characterized

by u parameter defined as $u = 0.25 + \left(d_{Cu-S}^2 - d_{Al-S}^2\right)/a^2$, where a is the lattice parameter in x and y direction. The second consequence of differing anion-cation bond lengths is a deformation of the unit cell along the z axis to a length c which is generally different from $2a$. This tetragonal distortion is characterized by the quantity c/a.

Table 1. The equilibrium lattice constants (a and c) (in Å), tetragonal distortion (c/a) and internal parameter (u) for $CuAlS_2$.

Method	a	c	c/a	u
Present work (VSSP-GGA)	5.344	10.534	1.971	0.258
VASP-GGA (Ref. [13])	5.362	10.526	1.963	0.259
ABINIT-LDA (Ref. [16])	5.239	10.415	1.988	0.255
WIEN2K-GGA (Ref. [36])	5.329	10.669	2.002	0.255
Exp. (Ref. [10])	5.335	10.440	1.957	0.255
Exp. (Ref. [37])	5.334	10.444	1.958	0.275
Exp. (Ref. [38])	5.334	10.444	1.958	0.268

The ground state equilibrium values of lattice constants (a and c), tetragonal distortion (c/a) and internal parameter (u) have been calculated by optimizing the total energy using first-principles calculations. The calculated values of these parameters are listed in Table 1 along with experimental [10,37,38] and calculated values [13,16,36]. Considering that the zero-point motion and thermal effects are not taken into account, the calculated lattice constants agree quite well with the experimental ones. Our calculations overestimate the equilibrium lattice parameter a (c) with the maximal error of 0.17-0.19% (0.86-0.90%) with respect to experimental values, a normal agreement by GGA standards. The value of u is slightly higher than the ideal value of 0.25 for all compounds of $A^IB^{III}C^{VI}_2$ chalcopyrite family except $AgInS_2$ and $CuInX_2$ (X=S, Se and Te) compounds, and agree well with the experimental value [10]. The optimized results show our calculation method is feasible and it is largely sufficient to allow the further study of vibrational and thermodynamic properties.

3.2. Phonon dispersion and density of states

Since the primitive unit cell of the chalcopyrite structure has eight atoms, there are a total of 24 modes of vibration. Group-theoretical analysis predicts the following irreducible representation for acoustical and optical zone-center modes:

$$\Gamma_{aco} = 1B_2 + 1E, \tag{3}$$

$$\Gamma_{opt} = 1A_1 + 2A_2 + 3B_1 + 3B_2 + 6E. \tag{4}$$

This gives rise 21 optical phonon branches which at the center of the BZ decompose into one A_1, two A_2, three B_1, three B_2 and six E. All these modes, except the A_2, are Raman (R) active, whereas only B_2 and E modes are infrared (IR) active. Both B_2 and E modes belong to vector

transforming representation, and inclusion of the long-rang polarization interaction results in splitting of these modes into TO and LO components giving nine polar vibrations.

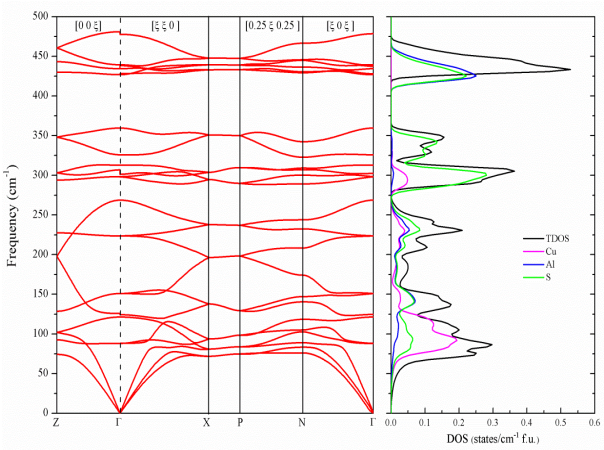

Fig. 2. Calculated phonon dispersion curves along symmetry lines in the BZ and the corresponding phonon density of states (DOS) for $CuAlS_2$.

The results for the phonon dispersion curves of $CuAlS_2$ along several high-symmetry lines together with the total and partial phonon densities of states are displayed in Fig. 2. The phonon DOS is normalized to the number of phonons with $\int_0^\infty g(\omega)d\omega = 1$. As can be seen from Fig. 2, the frequency range of atomic vibrations in $CuAlS_2$ is in accord with the typical 50-500 cm^{-1} for the $A^IB^{III}X_2^{VI}$ and $A^{II}B^{IV}X_2^{V}$ compounds [39]. The vibrational branches have significant dispersion except for the six almost flat branches at about 430 cm^{-1} forming a separate narrow band which corresponds to the strong peak in the DOS of this crystal. Our calculated zone-center phonon frequencies and their symmetry assignments are displayed and compared with Raman [6,7,9,10] and infrared [7,8] spectroscopic measurements and other theory values [16] in Table 2. Overall, the calculated zone-center phonon frequencies for $CuAlS_2$ are in agreement with experimental data. The calculation results of vibrational properties can ensure the accuracy of thermodynamic properties.

Table 3. A comparison of calculated phonon frequencies (in cm^{-1}) at the Γ point with Raman and infrared data as well as with other theory values. Two numbers in a row correspond to LO/TO frequencies.

Mode		Theory Present	Theory Ab initio[16]	Experiment IR[7]	IR[8]	R[9]	R[7]	R[10]	R[6]
A_1	R	326	325	—	—	315	316	314	315
A_2	Silent	313	304	—	—	—	—	—	—
	Silent	360	366	—	—	—	—	—	—
B_1	R	121	115	—	—	98	102	96	98
	R	269	263	—	—	268	269	263	268
	R	439	448	—	—	440	443	442	—

Mode		Theory Present	Theory Ab initio[16]	Experiment IR[7]	IR[8]	R[9]	R[7]	R[10]	R[6]
B_2	R, IR	126/124	120/119	—/114	111/105	111/111	—/114	108/108	112/112
	R, IR	298/298	296/287	—/271	285/264	270/270	—/267	—/272	278/266
	R, IR	481/438	495/453	—/446	500/456	495/456	—/446	498/446	497/445
E	R, IR	88/88	83/83	77/77	—	78/78	78/78	76/74	76/76
	R, IR	151/151	146/146	140/140	—	150/150	142/142	135/135	—
	R, IR	224/224	218/218	217/216	220/208	220/220	220/218	218/218	219/218
	R, IR	307/298	290/287	266/263	242/228	266/266	267/265	263/261	265/262
	R, IR	428/427	440/436	—/432	434/430	420/373	—/433	—	—
	R, IR	478/435	489/446	497/444	496/452	495/444	499/444	496/444	494/445

3.3. Thermodynamic properties

Based on QHA, we can obtain Helmholtz free energy (F), entropy of vibration (S), and specific heat at constant volume (C_V) at finite temperature from phonon DOS with various lattice volumes (V). Fig. 3 shows the variation of the Helmholtz free energy as a function of the lattice volume computed within the QHA with DFPT from 0 to 1000 K by step of 100 K. A lattice volume with minimum free energy was determined from fitting curves of the third-order Birch-Murnaghan equation of states [40]. Minimum energy points are connected by a red dashed line in Fig. 3. As shown in this figure, the lattice volume becomes larger with increase of temperature; hence the equilibrium volume changes at each given temperature.

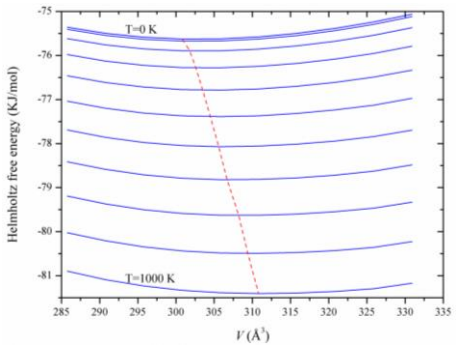

Fig. 3. Helmholtz free energy as a function of the lattice volume from 0 to 1000 K at every 100 K. Solid lines are F-V fitting curves according to the third-order Burch-Murnaghan equation of states. The local minimum of each free energy curve is indicated by a red dashed line.

The volume thermal expansion α_V can be indirectly reproduced by QHA without taking anharmonicity into account. To have an overall comparison of the thermal expansion, the coefficients of volume thermal expansion, defined by

$$\alpha_V = \frac{1}{V}\left(\frac{\partial V}{\partial T}\right)_P = \frac{1}{B}\left(\frac{\partial P}{\partial T}\right)_V, \quad (5)$$

where we have introduced the isothermal bulk modulus $B \equiv -V\left(\partial P / \partial V\right)_T$. The temperature dependences of the α_V are presented in Fig. 4. It is seen that for $CuAlS_2$ the coefficient α_V varies with temperature. At higher temperatures, the temperature dependence of thermal expansion coefficients is far weaker. The variation trend is consistent with the experimental results measured by Bodnar et al. [41]. Bulk modulus *B* can be obtained from the *F*-*V* fitting curve according to the third-order Birch-Murnaghan equation of states as shown in Fig. 5. We find that the bulk modulus *B* is nearly a constant at low temperature, whereas *B* decreases dramatically with the increment of temperature. Roa et al. [42] reported *B* of (99 ± 3) GPa at 300 K for $CuAlS_2$ using X-ray diffraction measurements. Our present calculations underestimated the experimental *B*. This is, however, a general trend for calculation with the GGA.

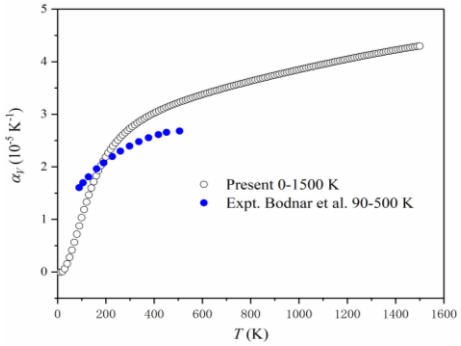

Fig. 4. The volume thermal expansion coefficient as a function of temperature.

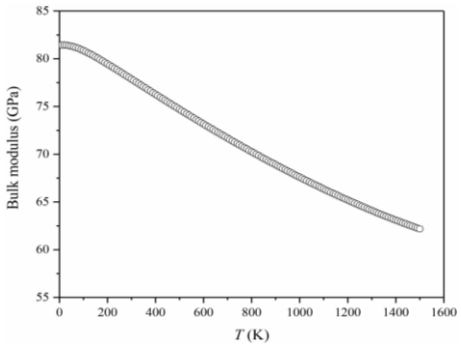

Fig. 5. The bulk modulus as a function of temperature.

The anharmonicity enables us to differentiate the heat capacity at constant volume C_V from the heat capacity at constant pressure C_P. The relation between C_V and C_P is

$$C_P - C_V = \alpha_V^2\left(T\right)BVT \tag{6}$$

and C_V is given by

$$C_V = 3nNk_B\int_0^{\omega_{\max}}\left(\frac{\hbar\omega}{2k_BT}\right)^2 \operatorname{csc}h^2\left(\frac{\hbar\omega}{2k_BT}\right)g\left(\omega\right)d\omega\,, \tag{7}$$

where n is the number of atoms per unit cell, N is the number of unit cells, ω is the phonon frequencies, $\omega_{\max}$ is the largest phonon frequency. Calculated C_V and C_P, together with the experimental and calculated results are presented in Fig. 6. In the low-temperature limit, the specific heat exhibits the T^3 power-law behaviour, and approaches at high temperature the classical asymptotic limit of $C_V=3nk_B=100$ J/mol K. The heat capacity at constant pressure C_P has been measured for $CuAlS_2$ in the temperature range from 80 to 300 K by Korzun et al. [26]. From the experimental results, Korzun et al. calculated the heat capacity at constant volume C_V. Moreover, the heat capacity at constant volume in the harmonic approximation C_{Vh} has been calculated using Debye model by Korzun et al. in the temperature range from 0 to 400 K. The calculated specific heat C_V and C_P of $CuInSe_2$ exhibit reasonable agreement with the experimental and other calculated values as shown in Fig. 6.

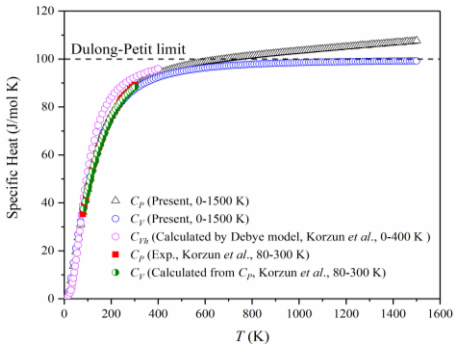

Fig. 6. The comparison between the calculated and experimental specific heat.

In the present study, the vibrational contribution to the entropy S was computed directly from phonon frequencies and DOS, obtained with DFPT at equilibrium volume, using the formulas

$$S = 3nNk_B \int_0^{\omega_{\max}} \left[\frac{\hbar\omega}{2k_BT} \coth \frac{\hbar\omega}{2k_BT} - \ln\left\{ 2\sinh \frac{\hbar\omega}{2k_BT} \right\} \right] \times g(\omega) d\omega . \qquad (8)$$

As shown in Fig. 7, the entropy S for $CuAlS_2$ calculated using equation (8) is in good overall agreement with values calculated using quasi-harmonic Deby model by Verma et al. [23]. The entropy for whole investigated interval of temperatures was calculated using the experimental results of C_P by Korzun et al. [26], defined by $\Delta S = S_{(T)} - S_{80} = \int_{80}^{T} C_p / T dT$. In order to better compare with the experimental results, we also calculated the values ΔS. As the temperature increases, the present calculations underestimated the experimental ΔS in the temperature range from 80 to 300K. At low temperatures from 80 to 110 K, the values ΔS predicted with DFPT are in excellent agreement with the experimental values.

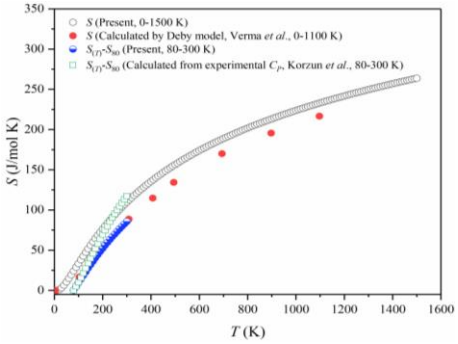

Fig. 7. The comparison between the calculated and experimental entropy.

4. Conclusions

The structural, vibrational and thermodynamic properties of ternary semiconductor $CuAlS_2$ were investigated from first-principles using density functional perturbation theory. Firstly, the structural parameters, including the internal coordinates, are relaxed, and excellent agreement is achieved with experimental results. The phonon dispersion curves of $CuAlS_2$ along several high-symmetry lines together with the total and partial phonon densities of states are calculated. All the Raman-active and infrared-active modes (including LO-TO splitting) are identified and compared with experiments and previous theoretical calculations. The calculated zone-center phonon mode frequencies are in good agreement with infrared, Raman and neutron scattering experiments. Finally, the thermodynamic properties including free energy, entropy, heat capacity and thermal expansion behavior are determined within the quasi-harmonic approximation based on the calculated phonon density of states. The calculated results are in good agreement with the experimental data in a wide range of temperature.

Acknowledgments

This work was supported by Scientific Research Fund of Sichuan Provincial Education Department (Grant No. 16ZB0209) and National Natural Science Foundation of China (Grant No. 11704049).

References

[1] H. J. Lewerenz, Sol. Energy Mater. Sol. Cells **83**, 395 (2004).
[2] M. Krunks, O. Kijatkina, A. Mere, T. Varema, I. Oja, V. Mikli, Sol. Energy Mater. Sol. Cells **87**, 207 (2005).
[3] K. Sato, K. Ishii, K. Watanabe, K. Ohe, Jpn. J. Appl. Phys. **30**, 307 (1991).
[4] S. Chichibu, S. Shirakata, S. Isomura, H. Nakanishi, Jpn. J. Appl. Phys. Part 1, **36**, 1703 (1997).
[5] M. Caglar, S. Ilican, Y. Caglar, Opt. Commun. **281**, 1615 (2008).
[6] W. H. Koschel, V. Hohler, A. Rauber, J. Baars, Phys. Stat. Sol. (b) **13**, 1011 (1973).

[7] W. H. Koschel, M. Bettini, Phys. Stat. Sol. (b) **72**, 729 (1975).
[8] A. M. Andrish, N. N. Syrbu, M. S. Iovu, V. E. Tezlevan, Phys. Stat. Sol. (b) **187**, 83 (1995).
[9] L. Roa, J. Gonzalez, J. C. Chervin, A. Chevy, Phys. Stat. Sol. (b) **211**, 429 (1999).
[10] B. H. Bairamov, A. Aydinli, I. V. Bodnar, Yu. V. Rud, V. K. Nogoduyko, V. V. Toporov, J. Appl. Phys. **80**, 5564 (1996).
[11] M. Bettini, W. B. Holzapfel, Solid State Commun. **16**, 27 (1975).
[12] R. O. Jones, O. Gunnarsson, Rev. Mod. Phys. **61**, 689 (1989).
[13] P. Hohenberg, W. Kohn, Phys. Rev. **136**, B864 (1964).
[14] S. Baroni, P. Giannozzi, A. Testa, Phys. Rev. Lett. **58**, 1861 (1987).
[15] S. Baroni S. de Gironcoli, A. Dal Corso, P. Giannozzi, Rev. Mod. Phys. **73**, 515 (2001).
[16] C. Parlak, R. Eryiğit, Phys. Rev. B **70**, 075210 (2004).
[17] J. Lazewski, K. Parlinski, B. Hennion, R. Fouret, J. Phys.: Condens. Matter **11**, 9665 (1999).
[18] Y. Yu, G. D. Zhao, X. L. Zheng, Z. R. Wei, Chalcogenide Lett. **13**, 15 (2016).
[19] M. Akdogan, R. Eryiğit, J. Phys:Condens. Matter **14**, 7493 (2002).
[20] C. Parlak, R. Eryiğit, Phys. Rev. B **73**, 245217 (2006).
[21] R. Eryiğit, C. Parlak, R. Eryiğit, Eur. Phys. J. B **33**, 251 (2003).
[22] Y. Yu, Y. J. Dong, Y. H. Shen, G. D. Zhao, X. L. Zheng, J. N. Sheng, Chin. Phys. B **26**, 046302 (2017).
[23] U. P. Verma, P. Jensen, M. Sharma, P. Singh, Comput. Theor. Chem. **975**, 122 (2011).
[24] M. A. Blonco, E. Frencisco, V. Luana, Comput. Phys. Commun. **158**, 57 (2004).
[25] P. Nath et al., Comp. Mater. Sci. **125**, 82 (2016).
[26] B. V. Korzun, R. R. Mianzelen, A. U. Sheleg, N. P. Tekhanovich, K. Bente, W. Schmitz, Phys. Stat. Sol. (b) **242**, 1990 (2005).
[27] A. Kuwabara, T. Tohei, T. Yamamoto, I. Tanaka, Phys. Rev. B **71**, 064301 (2005).
[28] T. Tohei, A. Kuwabara, F. Oba, I. Tanaka, Phys. Rev. B **73**, 064304 (2006).
[29] T. Tohei, H.-S. Lee, Y. Ikuhara, Mater. Trans. **56**, 1452 (2015).
[30] G. Kresse, J. Furthmuller, Phys. Rev. B **54**, 11169 (1996).
[31] G. Kresse, D. Joubert, Phys. Rev. B **59**, 1758 (1999).
[32] J. P. Perdew, Y. Yang, Phys. Rev. B **45**, 244 (1992).
[33] C. Lee, W. Yang, R. G. Parr, Phys. Rev. B **37**, 785 (1988).
[34] J. P. Perdew, Y. Wang, Phys. Rev. B **45**, 13244 (1992).
[35] A. Togo, F. Oba, I. Tanaka, Phys. Rev. B, **78** (2008) 134106.
[36] A. Ghosh, R. Thangavel, M. Rajagopalan, J. Mater. Sci. **50**, 1710 (2015).
[37] H. W. Spiess, U. Heaberln, G. Brandt, A. Rauber, J. Schneider, Phys. Stat. Sol. (b) **62**, 183 (1974).
[38] G. Brandt, A. Bauber, J. Schneider, Solid State Commun. **12**, 481 (1973).
[39] F. W. Ohrendorf, H. Haeuseler, Cryst. Res. Technol **34**, 339 (1999).
[40] J. P. Poirier, Introduction to the Physics of the Earth's Interior, 2nd ed. (Cambridge University Press, New York, 2000).
[41] I. V. Bodnar, N. S. Orlova, Phys. Stat. Sol. (a) **78**, K59 (1983).
[42] L. Roa, J. C. Chervin, J. P. Itie, A. Polian, M. Gauthier, A. Chevy, Phys. Stat. Sol. (b) **211**, 455 (1999).